

FLUXON-INDUCED LOSSES IN NIOBIUM THIN-FILM CAVITIES REVISITED

W. Weingarten*

Abstract

Long standing data from niobium thin film accelerating cavities will be revisited and analysed by the two-fluid model of RF superconductivity. Firstly, the applicability and limitation of this model are explored using data of the BCS surface resistance and its dependence on the RF magnetic field, temperature and mean free path. Secondly, the RF losses from trapped magnetic flux are analysed with regard to their dependence on these same parameters.

INTRODUCTION

The two-fluid model of Gorter and Casimir [1] was extended by Fritz and Heinz London for RF applications [2], many years before the Bardeen-Cooper-Schrieffer (BCS) theory of superconductivity [3] was published. The two-fluid model describes the Meissner effect [4] and also, though in a qualitative way, the surface resistance R_s of classical superconductors (cf. eq. 1).

The surface resistance R_s , or equivalently, the Q-value ($R_s \sim Q^{-1}$), are important parameters for accelerator application with respect to cryogenic losses and beam stability [5]. Therefore, in this paper, the two-fluid model will be applied to debate the RF field dependence of the Q-value on trapped magnetic flux of a 1.5 GHz niobium coated copper cavity by using data from Benvenuti et al. [6]. The present analysis also constitutes a follow-up of, and a complement to, a previously published study [7].

The paper is organized as such: in the *first* section the two-fluid model is applied using data of the RF field dependent BCS surface resistance versus temperature and mean free path. In the *second* section the relation of the surface resistance on trapped magnetic flux will be analysed, both for the RF field independent and the RF field dependent part. The *third* section deals with the trapped magnetic flux induced surface resistance vs. temperature.

THE RF-FIELD DEPENDENCE OF THE BCS SURFACE RESISTANCE ON TEMPERATURE AND MEAN FREE PATH

As a first test the data on the BCS-surface resistance R_{BCS} will be analysed to gain confidence in the two-fluid model approach. We start with eq.1, adopted from [8], and supplemented by the linear term αB_{rf} , as suggested by ref. 6:

$$R_{BCS}(\omega, T) = \mu_0^2 \omega^2 \lambda^3 \sigma_n \frac{\Delta}{k_B} \overbrace{\ln\left(\frac{\Delta}{\hbar\omega}\right) \frac{e^{-\frac{\Delta}{T}}}{T}}^{f'(T)} (1 + \alpha B_{rf} + \beta B_{rf}^2); B_c = 1/\sqrt{2\beta}. \quad (1)$$

The symbols are the peak RF magnetic field B_{rf} , the magnetic constant μ_0 , the frequency $\omega/(2\pi)$, the penetration depth λ , the electrical conductivity σ_n of the normal conducting (nc) electrons at low temperature, their temperature dependence $f'(T)$ in the superconducting (sc) state, the Boltzmann constant k_B , and the sc energy gap Δ . The (coloured) curves as shown in Fig. 1 follow from eq. 1 with the fit parameters as of Table 1. The critical magnetic field $B_c = 183$ mT (or $\beta = 1.5 \cdot 10^{-5} (\text{mT})^{-2}$, resp.) is kept fix.

Table 1: Fit parameters with regard to Fig.1

$\omega/(2\pi)$ [GHz]	λ [nm]	σ_n [1/(Ωm)]	Δ [K]	α [1/(mT)]
1.5	40	$1.53 \cdot 10^8$	18.9	$7.5 \cdot 10^{-3}$

The intrinsic parameters of niobium are the London penetration depth $\lambda_L = 32$ nm, the coherence length $\xi_0 = 33$ nm, and the electrical conductivity at room temperature $\sigma_{n,300\text{K}} = 7.6 \cdot 10^6 (\Omega\text{m})^{-1}$. These parameters imply a residual resistivity ratio $RRR = 20$, and an electron mean free path $l = 2.85 \cdot RRR = 57$ nm.

* retiree from CERN, Geneva, Switzerland (wolfgang.weingarten@cern.ch)

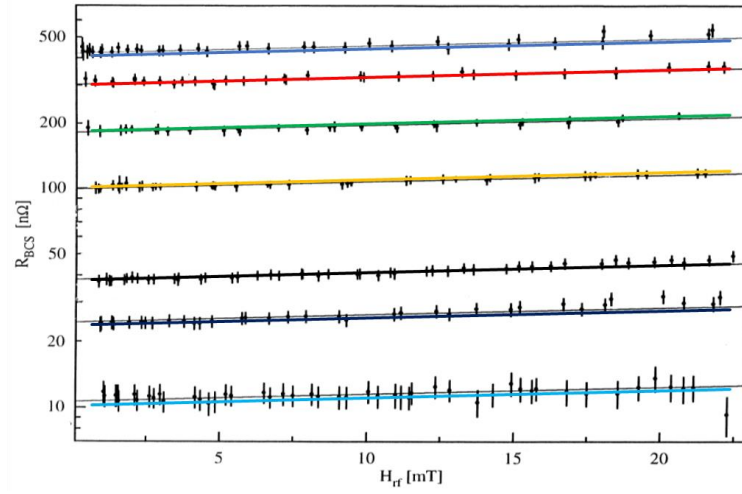


Fig. 1: The BCS-surface resistance R_{BCS} of a thin niobium film cavity as a function of the magnetic peak RF field H_{rf} for different temperatures (from top to bottom at 4.23, 3.9, 3.47, 3.07, 2.59, 2.41, and 2.15 K). Superimposed *in coloured lines* is a least square fit as suggested by eq. 1. The data are taken from ref. 6.

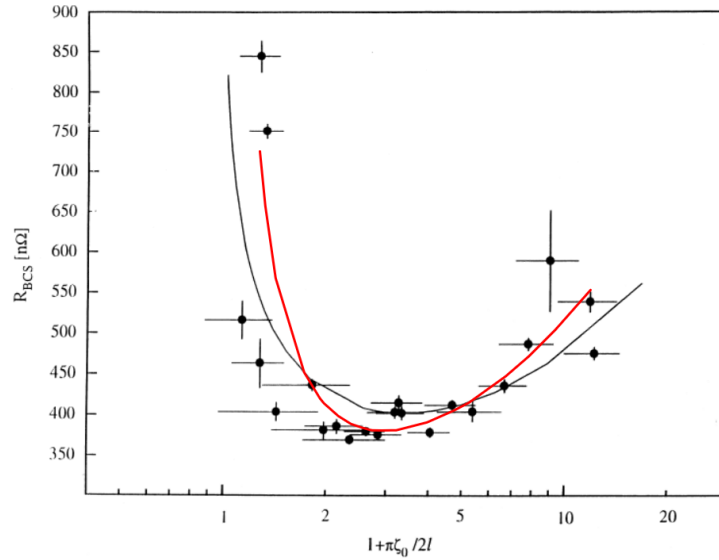


Fig. 2: BCS surface resistance vs. the relative penetration depth $(\lambda/\lambda_L)^2$. The continuous line (red) is calculated from eq. 1 and superimposed on the data from ref. 6.

As a second test, the data on R_{BCS} from ref. 6 are shown versus the square of the relative penetration depth: $\lambda_{\text{rel}}^2 = (\lambda/\lambda_L)^2 = 1 + \pi \cdot \zeta_0 / (2 \cdot l)$. Superimposed is the result as derived from eq. 1. Here the relevant parameters are $T = 4.2$ K, $\sigma_{n,300\text{K}} = 7.6 \cdot 10^6 (\Omega\text{m})^{-1}$, and $\Delta = 19.5$ K. The characteristic minimum is clearly visible at $\lambda_{\text{rel}}^2 = 3$ which corresponds to $l = 27$ nm.

Eq. 1 was also checked against the data of Fig. 2 with $f'(T)$ of eq. 1 replaced by $f'(T) = (T/T_c)^4$ from the original two-fluid model, T_c being the critical temperature of niobium (the temperature dependence of λ is neglected near 4.2 K). In this case R_{BCS} is underestimated by approximately one order of magnitude. Hence, whenever temperature unrelated issues are concerned, the two-fluid model is considered as a trustful tool for data analysis.

THE DEPENDENCE OF THE SURFACE RESISTANCE ON TRAPPED MAGNETIC FLUX

The niobium thin film cavities developed at CERN are less sensitive to DC trapped magnetic flux B when cooled down. The small dependence of the magnetically induced surface resistance R_{fl} on B and B_{rf} can be parametrized as [6]

$$R_{fl} = (R_{fl}^0 + R_{fl}^1 \cdot B_{rf}) \cdot B \quad , \quad (2)$$

which is composed of the RF-field independent and the RF-field dependent fluxon sensitivities R_{fl}^0 and R_{fl}^1 , measured in nΩ/Gauss and nΩ/Gauss/mT, resp.

The losses from R_{fl}^0 may be understood by the voltage created from the inertia of the sc shielding current \mathbf{j} which develops across the nc core of the trapped fluxons, as derived in ref. 7 (c.f. appendix). The current flows via two parallel impedances, one a resistance, the other an inductance. Nonetheless, ref. 7 merits to be revisited, because the postulated data for the upper critical field B_{c2} of niobium are debateable and the RF magnetic field dependent contribution to the surface resistance R_{fl}^1 is not yet treated.

The RF field independent contribution R_{fl}^0

There are two contributions to the RF field independent surface resistance R_{fl}^0 . In all what follows, the fluxons are considered to move freely, their depinning frequency being much smaller than the RF frequency (1.5 GHz) [9].

The **first contribution** is attributed to fluxons directly exposed to the RF shielding current $\mathbf{j} = (j_x, 0, 0)$.

As outlined in the appendix,

$$R_{fl}^0 = (\omega\mu_0)^{3/2} (2\sigma_n)^{1/2} \lambda^2 \frac{1}{B_{c2}} \quad . \quad (3)$$

The **second contribution** is attributed to fluxons (indirectly) exposed to an inductive current. It is well known that an RF current density $\mathbf{j} = (j_x, 0, 0)$ flowing perpendicular to a *static magnetic* field $\mathbf{B} = (0, B_y, 0)$ will create the Lorentz force density on the fluxon $\mathbf{F} = (0, 0, F_z) = \mathbf{j} \times \mathbf{B}$ that will move it with the velocity $\mathbf{v} = \eta^{-1} \cdot \mathbf{F}$ (c.f. Fig. 3 and Table 2).

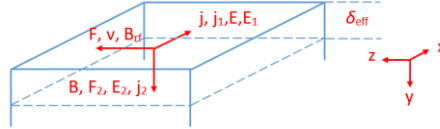


Fig. 3: Geometry as referred to in the text (*the letters indicate to which axis the different vectors are parallel; they do not indicate their direction*)

The moving fluxon induces an electric field $\mathbf{E} = (E_x, 0, 0) = \mathbf{B} \times \mathbf{v}$ that will create a current density $\mathbf{j}_1 = (j_{1x}, 0, 0) = (E_{1x}/\rho_n, 0, 0)$; ρ_n is the electrical resistivity of the nc electrons at low temperature.

The current \mathbf{j}_1 acts on the nc electrons in a similar way as the current \mathbf{j} , but in quadrature. Hence \mathbf{j}_1 contributes identically to the fluxon induced surface resistance R_{fl}^0 . The reason is that the force \mathbf{F} is in phase with \mathbf{j} , as is the velocity \mathbf{v} . But by induction, \mathbf{v} induces an electric field \mathbf{E}_1 in quadrature to \mathbf{j} . As consequence from Fig. 12, the different power dissipations P and P_1 due to \mathbf{j} and \mathbf{j}_1 (or equivalently I and I_1 respectively), may be added: $P = \frac{1}{2} R (I + iI_1) \cdot (I - iI_1) = \frac{1}{2} R I^2 + \frac{1}{2} R I_1^2 + \frac{1}{2} i \cdot R \cdot I \cdot I_1 - \frac{1}{2} i \cdot R \cdot I_1 \cdot I = P + P_1$. So do the respective surface resistances $R_s = E/(\lambda \cdot j) = E_1/(\lambda \cdot j_1)$. Hence R_{fl}^0 is composed of twice the value of eq. 3.

Table 2: Used symbols and their definition [10]

Physical quantity	Symbol	Unit
Shielding current density	$\mathbf{j} = \mathbf{E}/\rho_n$ ¹⁾	A/m ²
Magnetic induction	\mathbf{B}	Vs/m ²
Lorentz force density	$\mathbf{F} = \mathbf{j} \times \mathbf{B}$	N/m ³
Vortex velocity	$\mathbf{v} = \eta^{-1} \mathbf{F}$ ²⁾	m/s
Electric field from moving fluxons	$\mathbf{E} = \mathbf{B} \times \mathbf{v} = \eta^{-1} \mathbf{B} \times (\mathbf{j} \times \mathbf{B}) = \rho_n \mathbf{j}$ ³⁾	V/m
Electric field from Lorentz force density	$\mathbf{E} = \mathbf{j} \times \mathbf{B}/(n \cdot e)$ ⁴⁾	V/m
Hall resistivity	$\rho_{yx} = E_y/j_x = R \cdot B$ ⁵⁾	Ωm

¹⁾ ρ_n is the normal state resistivity at low temperature; ²⁾ η is the drag coefficient; ³⁾ $\rho_n \approx (B/B_{c2}) \rho_n$ [11];
⁴⁾ n is the normal state electron density; ⁵⁾ $R = 1/(n \cdot e)$ is the Hall coefficient

The fluxon sensitivity R_{fl}^0 is equivalent to the DC result for the “ideal” material as outlined by Gittleman and Rosenblum [9]. However, R_s is too large as to represent the data of ref. 6, because, as supposed, the RF current does not entirely flow through the nc core, as supposed by eq. 4, but partially avoids it.

In order to make use of eq. 3, data of B_{c2} for representative thin films similar to those grown on the cavity surface are collected from the literature (Table 3).

These data are plotted in Fig. 4 in conjunction with data on bulk niobium samples [12, 13] (dashed lines). The by-eye-averaged line of thin film data is used in the following analyses (marked as “average”).

Applying the average data (Fig. 4) to eq. 3 results in the red solid curve of the trapped fluxon sensitivity R_{fl}^0 as of Fig. 5. The relevant parameters are the electrical conductivity at low temperature $\sigma_{n,300\text{K}} = 7.6 \cdot 10^6 \text{ (}\Omega\text{m)}^{-1}$, $\lambda_L = 32 \text{ nm}$, $\zeta_0 = 33 \text{ nm}$, and $l \text{ [nm]} = 2.85 \cdot RRR$.

Table 3: Data of B_{c2} for sputtered niobium films

Film thickness [μm]	$B_{c2, 4.2 \text{ K}}$ [kGauss]	RRR	Mean free path $l \text{ [nm]} = 2.85 \cdot RRR$	Reference
5	20	15	43	adopted from ref. 7
3.7	21	6.7	19	
3	15	13	37	
3	26	9	26	
1.6 – 1.8	28	12	34	
1.5	8.5	11.5	33	[14]
1.5	5.5	29	83	[15]
0.1	36 ^{*)}	1.1	3.2	
0.1	8 ^{*)}	22.8	65	
0.1	34 ^{*)}	1.4	3.9	

*) Numbers were extrapolated to 4.2 K

The agreement with the published data of ref. 6 is satisfactory and the trend of the curve is well represented. It should be noted that this curve was obtained by taking into account the variation of the trapped flux density across the cavity surface. The average flux density is by a factor 1.6 smaller (for the static magnetic field parallel to the cavity axis) as compared to a fictitious maximum flux density when all surface were exposed to the *perpendicular* component of the static magnetic field [16]. This correction shifts the curve slightly down and will be applied in what follows, too. Principally unknown is the trapping efficiency, but from experiment it is known to be close to one [17].

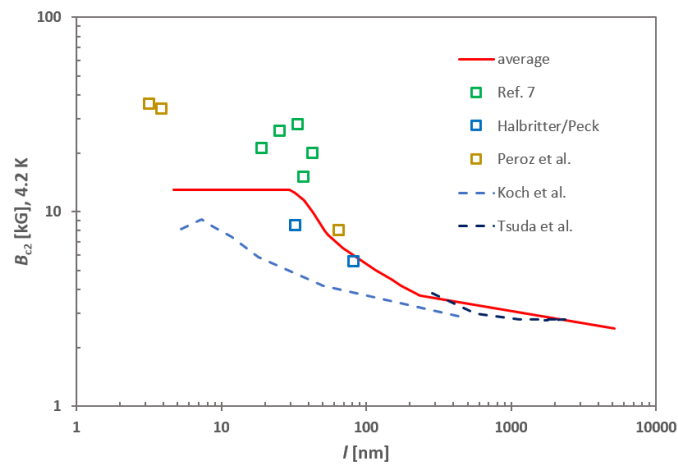


Fig. 4: Upper critical magnetic field B_{c2} of samples of niobium thin films (*squares*) and bulk (*dashed lines*) vs. mean free path (derived from their RRR value). The red *solid* line represents “averaged” thin film data.

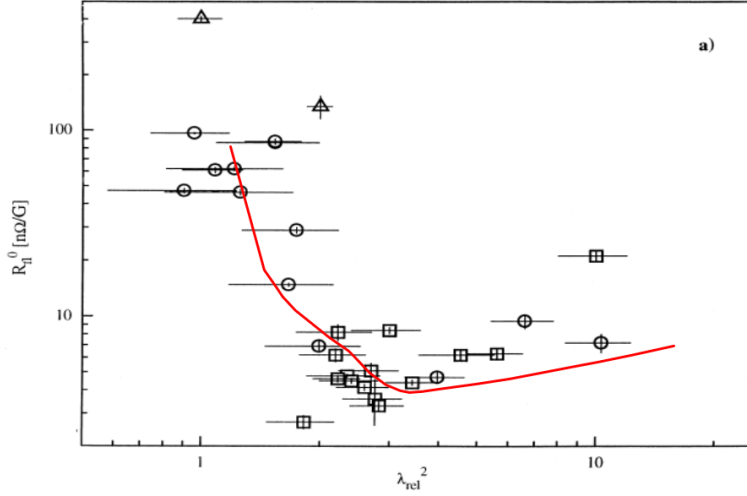


Fig. 5: Trapped fluxon sensitivity R_n^0 vs. the square of the relative penetration depth $(\lambda/\lambda_L)^2$. The continuous line (red) is calculated from eq. 3 (but multiplied by factor 2, as explained in the text) using the “averaged” data for B_{c2} and is superimposed on the data from ref. 6.

A different check of the model is provided by the dependence of the fluxon sensitivity R_n^0 on the RF frequency. The data are obtained from Calatroni and Vaglio [18] and reproduced in Table 4 and in Fig. 6.

The first three lines are measured for bulk niobium, while the two bottom lines for niobium films on copper.

Table 4: Magnetic flux sensitivities R_n^0 and R_n^1 as measured by several authors.

Reference	Frequency [MHz]	R_n^0 [nΩ/G]	R_n^1 [nΩ/G/mT]
Piosczyk [19]	91/160/290	3.5/9.5/28	0.35/0.55/0.9
Arnolds-Mayer [20]	500	150	5
Checchin [21]	650/1300/2600/3900	700/1000/1500/1900	1.6/2.6/6.1/7.4
Miyasaki [22]	101	3.2	0.32
Benvenuti [23]	1500	3.3/56	0.91/4.5

Although the data on R_n^0 were collected for a variety of experimental conditions, niobium metals, processing techniques, and in different laboratories, etc., they are not in contradiction with the expected frequency dependence ($\sim \omega^{3/2}$) of R_n^0 , c.f. eq. 3.

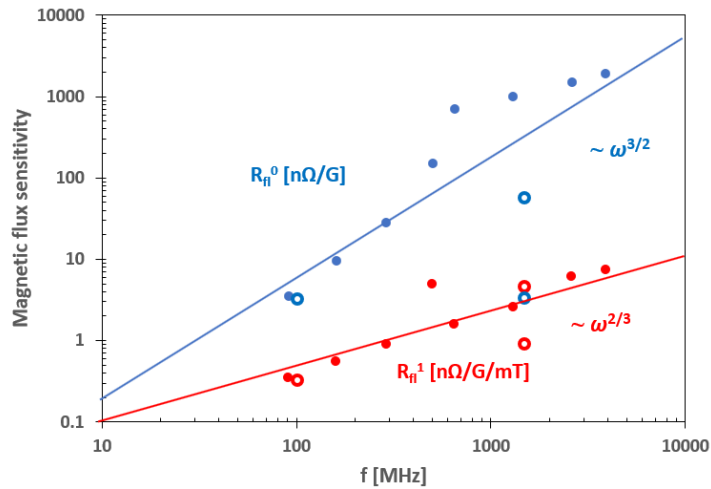


Fig. 6: Frequency dependence of the fluxon sensitivities R_n^0 and R_n^1 (full dots: bulk niobium; open dots: niobium film)

The RF field dependent contribution R_n^1

The RF field dependent part of the fluxon sensitivity R_n^1 is actually under study by different authors [18] and is also observed in niobium bulk cavities [24] as well as in those undergone N-doping treatment [25].

The role of the anomalous skin effect

The skin effect is created by surface currents in the metal which short-circuit the electric field parallel to the surface. The domain of the anomalous skin effect is at low temperatures, where the mean free path l of the electrons gets larger than the penetration depth. Only electrons whose mean free path l ranges within a surface layer where a non-vanishing electric field is present (the effective penetration depth δ_{eff}) contribute to the current shielding the external RF field. The others are “invisible” to the electric field (Fig. 7) [26].

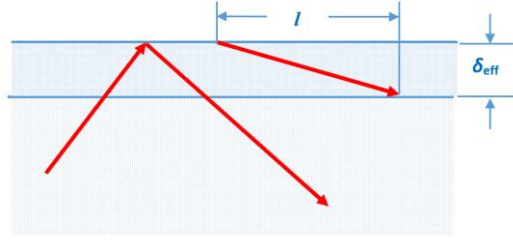


Fig. 7: Only electrons within the effective penetration depth contribute to shielding the external RF field.

Hence the effective density of the electrons is reduced by the factor $\alpha \cdot \delta_{\text{eff}}/l$ with $\alpha \approx 1$. The effective conductivity is, therefore, given by $\sigma_{\text{eff}} = \alpha \cdot \delta_{\text{eff}}/l \cdot \sigma_n$. Introducing this into the formula for the skin depth, $\delta = \sqrt{2/(\mu_0 \cdot \sigma_n \cdot \omega)}$, one obtains

$$\delta_{\text{eff}} = \left(\frac{2 \cdot l}{\alpha \cdot \mu_0 \cdot \sigma_n \cdot \omega} \right)^{1/3}, \quad (4)$$

$$\sigma_{\text{eff}} = \left(\frac{2}{\mu_0 \cdot \omega} \right)^{1/3} \left(\frac{\alpha \cdot \sigma_n}{l} \right)^{2/3}. \quad (5)$$

Similarly, the effective surface resistance is $R_{s,\text{eff}} = 1/(\sigma_{\text{eff}} \cdot \delta_{\text{eff}})$, which exhibits the characteristic frequency dependence ($\sim \omega^{2/3}$) of the surface resistance in the anomalous limit.

The role of the Hall effect

The observed frequency dependence of R_n^1 ($\sim \omega^{2/3}$) as of Fig. 6 already points to the anomalous skin effect as relevant for R_n^1 .

It is observed that there exists a different electric field, the Hall field $\mathbf{E}_2 = (0, E_{2y}, 0)$, cf. Fig. 3, created by the Lorentz force density $\mathbf{F}_2 = (0, F_{2y}, 0) = \mathbf{j} \times \mathbf{B}_{\text{rf}} = (j_x, 0, 0) \times (0, 0, B_{\text{rf},z})$. The electrons feel the force $e\mathbf{E}_2 = \mathbf{F}_2/n = \mathbf{j} \times \mathbf{B}_{\text{rf}}/n$, n being the electron density. This force creates the current $\mathbf{j}_2 = (0, j_{2y}, 0)$ with $j_{2y} = \sigma_{yx} \cdot E_x = E_x/(B_{\text{rf},z} \cdot R) = n \cdot e/B_{\text{rf},z} \cdot \rho_n \cdot j_x$, $R = 1/(ne)$ being the Hall coefficient (cf. Table 2). The RF losses per volume and electron are then $P = \langle \mathbf{E}_2 \cdot \mathbf{j}_2 \rangle = 1/2 \cdot \rho_n \cdot j_x^2$. With $j_x = H_{\text{rf}}/\lambda$ follows for the power loss per square meter p :

$$p = P \cdot \lambda = \frac{1}{2} \cdot \frac{\rho_n}{\lambda} \cdot H_{\text{rf}}^2.$$

With the surface fraction of fluxons B/B_{c2} (cf. appendix), one obtains

$$p = \frac{1}{2} \cdot \frac{\rho_n}{\lambda} \cdot H_{\text{rf}}^2 \cdot \frac{B}{B_{c2}} = \frac{1}{2} \cdot R_{fl}^1 \cdot H_{\text{rf}}^2 \cdot B_{\text{rf}} \cdot B,$$

resulting in

$$R_{fl}^1 = \frac{\rho_n}{\lambda \cdot B_{\text{rf}} \cdot B_{c2}}. \quad (6)$$

Eq. 6 is now evaluated under similar parameters as for eq. 3, however with two distinctions. The first distinction is governed by the anomalous skin effect with the mean free path $l > \lambda$. Hence the replacements $\rho_n \rightarrow 1/\sigma_{\text{eff}}$ and $\lambda \rightarrow \delta_{\text{eff}}$ from eqs. 4 and 5 are inserted in eq. 6. The second distinction follows as such:

$$R_{fl}^1 = \frac{\rho_n}{\lambda \cdot B_{rf} \cdot B_{c2}} = \frac{1}{\sigma_n \cdot \lambda \cdot B_{rf} \cdot B_{c2}} = \frac{m}{n \cdot e^2 \cdot \tau \cdot \lambda \cdot B_{rf} \cdot B_{c2}} = \frac{1}{n \cdot e \cdot \tau \cdot \lambda \cdot \omega_c \cdot B_{c2}} = \frac{1}{n \cdot e \cdot l \cdot B_{c2}} \quad (7)$$

(cyclotron frequency $\omega_c = eB_{rf}/m$, electrical conductivity $\sigma_n = ne^2\tau/m$, effective electron mass m , electron density n , electric charge e , collision time τ). The mean free path l is the typical length the electron can go without being scattered.

In both cases the electrical conductivity σ and the electron density n are kept fixed at 17 % their room temperature value ($\sigma_n = 0.17 \cdot \sigma_{n,300\text{ K}}$; $\sigma_{n,300\text{ K}} = 7.6 \cdot 10^6 (\Omega\text{m})^{-1}$; $n = 0.17 \cdot n_0$; $n_0 = 5 \cdot 10^{28} \text{ m}^{-3}$). This is in order to allow for disordered niobium [27] or niobium alloys considered to establish the fluxon pinning centre. These provisions result in the graph of Fig. 8, where the two distinctions are marked as dashed lines (left: $l > \lambda$; right: $l < \lambda$). The left branch with $l > \lambda$ shows the characteristic frequency dependence of R_{n1}^1 , as characteristic for the anomalous skin effect for bulk niobium ($\sim \omega^{2/3}$), in accordance with Fig. 6.

Combination of R_{n0} and R_{n1}^1

As a check of the results obtained so far, Fig. 9 from ref. 6 displays the combined fluxon sensitivity as in eq. 2. The red line is superimposed by fitting these data with the parameters $R_{n0} = 4.7 \text{ n}\Omega/\text{G}$ and $R_{n1}^1 = 1.0 \text{ n}\Omega/\text{G/mT}$. These numbers are consistent with Figs. 5 and 8.

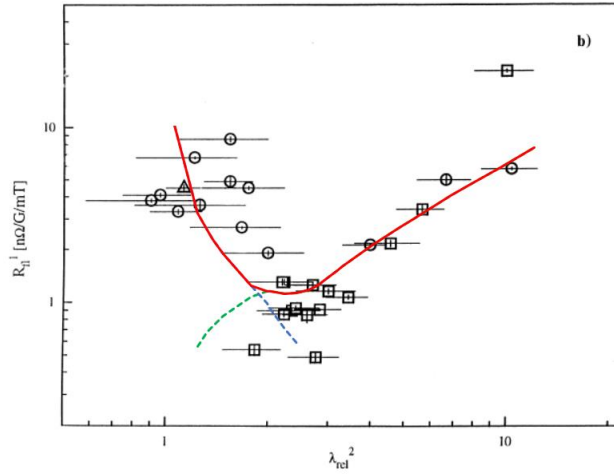


Fig. 8: Trapped fluxon sensitivity R_{n1}^1 vs. the square of the relative penetration depth $(\lambda/\lambda_L)^2$. The continuous line (red) is the combination of the two dashed lines (blue and green), as calculated from eqs. 6 and 7, and superimposed on the data from ref. 6.

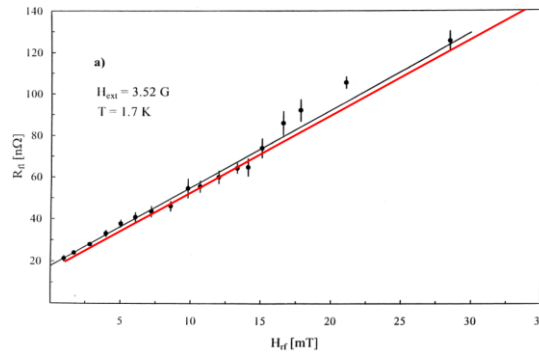


Fig. 9: Combined fluxon sensitivity vs. the RF magnetic field at an external magnetic field 3.52 Gauss (adapted from ref. 6).

The data from Figs. 5 and 8 (continuous line) and eqs. 3, 6 and 7 are correlated as shown in Fig. 10.

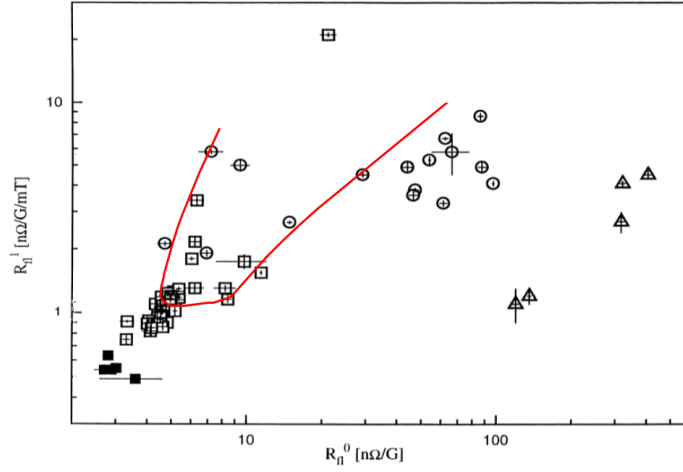


Fig. 10: Correlation of R_n^1 vs. R_n^0 (data adopted from ref. 6)

THE DEPENDENCE OF THE TRAPPED MAGNETIC FLUX INDUCED SURFACE RESISTANCE ON THE TEMPERATURE

Eqs. 3 and 7 show that the fluxon sensitivity depends on $B_{c2}(T)$ and $\lambda(T)$. For the penetration depth λ the standard relation is used,

$$\lambda = \lambda_L \cdot \frac{\sqrt{1 + \frac{\pi \xi_0}{2l}}}{\sqrt{1 - \left(\frac{T}{T_c}\right)^4}} \quad (8)$$

For $B_{c2}(T)$ the relation $B_{c2} [T] = 4 \cdot (1 - T [K]/9.25)$ as presented in Fig. 4 of ref. 28 is applied, though with the caveat that $B_{c2}(T)$ for the present data is unknown.

The data to be analysed are shown in Fig. 11, which displays the ratio $r = R_n(T)/R_n(1.7 \text{ K})$, as defined in ref. 6. According to ref. 6 this graph is quite universal and independent of the specific choice of B_{rf} and B . The ratio r was measured at identical values of B_{rf} and B and then displayed as a function of the temperature. The continuous line in Fig. 11 was computed by means of eqs. 3 and 7 with the usual parameters as of the graph in Fig. 4 with $RRR = 20$ and $B_{rf} = 5 \text{ mT}$.

The analysis allows concluding that Fig. 11 reflects mainly the relatively strong dependence on the temperature T of R_n^0 because the penetration depth λ as of eq. 8 is supposed to increase steeply above about 4.5 K. The dependence on T of R_n^1 , on the contrary, is weak up to 4.2 K consequent to the relatively weak dependence of B_{c2} on T .

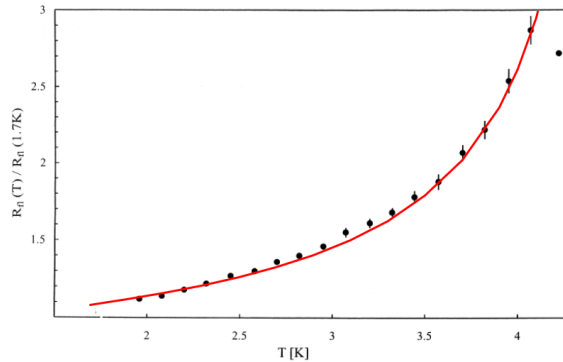


Fig. 11: Increase of the ratio r of the fluxon sensitivity vs. temperature. The continuous line (red) is calculated from eqs. 3 and 7 and superimposed on the data from ref. 6.

CRITICAL REVIEW

Admittedly the preceding analysis is based on a few deficiencies, such as the scarce knowledge of B_{c2} for thin films in general and for the data analysed here in particular. In addition, the actual trapping efficiency of the magnetic flux is unknown though considered as fairly complete from similar other experiments. In spite of these fragmentary information, the most interesting outcome from this analysis is the fact that the observed RF losses can be best described by

- fluxons with local critical temperature around 4.5 K and a reduced electron density, compared to standard niobium,
- localized RF losses originating inside and in close vicinity of these fluxons,
- created by the moving fluxons and the local Hall field directed perpendicular to the current carrying surface, and
- the anomalous skin effect (for mean free paths larger than the penetration depth) due to the ineffectiveness of the shielding current.

That the RF losses are concentrated around, and dominated by, the fluxons is not surprising, because the surface resistance from different cavity wall areas is additive and hence naturally dominated by the lossiest areas. The associated local critical temperature may hint on dirty and/or disordered niobium rich with dislocations, or on dissolved oxygen near the solubility limit. It is evident that the external static magnetic field will preferentially be trapped precisely there.

CONCLUSION

In this paper the two-fluid model of RF superconductivity allows quantifying the RF losses in sc niobium thin film cavities originating from trapped fluxons, considered as being depinned and hence mobile at the RF frequency under study (1.5 GHz).

The RF losses from trapped fluxons consist of two contributions, those *directly* exposed to the RF shielding current and those *indirectly* exposed to the RF inductive current. The directly exposed fluxons experience RF losses similar to nc defects across the current path. The indirectly exposed fluxons contribute to the RF losses in two ways. Firstly, they create a current in quadrature but parallel to the shielding current and hence give rise to the same additive surface resistance as the latter. Secondly, they create an RF Hall current perpendicular to the surface and confined within the small penetration depth, also dissipating energy in the fluxons. A model in accordance with these explanations corroborates the experimental facts of ref. 6: the surface resistance for both species of current increases linearly with the fluxon density, and that due to the Hall current increases linearly with the RF field amplitude. The minimum surface resistance from trapped fluxons is associated with RRR about 9 to 18.

ACKNOWLEDGEMENT

The autor warmly thanks Sergio Calatroni (CERN) for valuable hints and suggestions.

APPENDIX

The lumped-circuit model of Fig. 12 shows an inductance L and a resistance R in parallel subject to the total current I . The inductance describes the sc electrons, the inertia of which give rise to a voltage V . The resistance describes the nc ones present in the superconductor, subject to the voltage V .

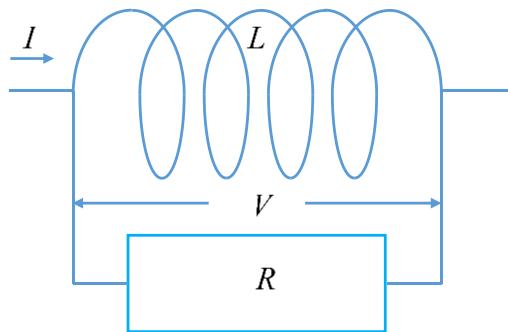


Fig. 12. Two-fluid model representation of the current flow through a superconductor.

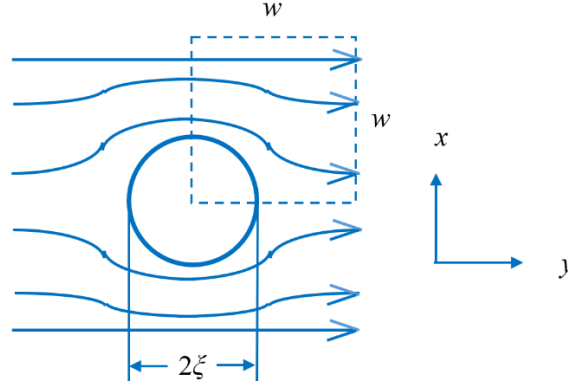


Fig. 13. Schematic current path around a fluxon: the current path is shown in plan view. The square of width w shows a quarter of the perturbed region of current due to the presence of the fluxon of diameter 2ξ . The current penetrates the paper plane perpendicularly a distance δ into the fluxon, yet the current penetrates the sc metal in the vicinity of the fluxon to a distance of λ .

We consider a square of a superconductor as shown in Fig. 13 with a current flowing partly through and partly past a fluxon. We want to calculate the surface resistance and the surface inductance of this slab of width w , which represents approximately the region of interest of one-quarter of a fluxon (Fig. 13) and the sc metal in the vicinity.

The RF losses for an individual fluxon are given by $P_{fl} = (1/2)RI_2^2$, where I_2 is the current through the fluxon (which is purely resistive) and R its resistivity. This current I_2 is determined by the total current I , $I_2 = I / \{1 + [R/(\omega L)]^2\}$, where L represents the inductance of the sc electrons in the vicinity of the fluxon. Hence, the losses per fluxon

$$P_{fl} = \frac{1}{2} \cdot R \cdot \frac{1}{1 + [R/(\omega L)]^2} \cdot I^2 \quad .$$

We shall now calculate the characteristic values for the different elements of the lumped circuit model. The resistance of the fluxon is determined by the conductivity σ_n and the nc penetration depth δ , $R \approx R_N = (\sigma_n \cdot \delta)^{-1}$. In this first-order approximation, the current flows perpendicularly to a square column of half-width instead of a cylinder of radius ξ . The inductance of the quadratic slab of width w (far away from the fluxon core) is determined by the definition of the voltage $V = -i\omega LI$, which is equal to $V = E_y w$. The Maxwell equation $\text{curl} \mathbf{E} = -d\mathbf{B}_{rf}/dt$ defines the electric field component $E_y = i\omega \lambda B_{rf,x}$, with the magnetic surface field $B_{rf,x}$. From the total current $I = B_{rf,x} w / \mu_0$, we obtain $L = \mu_0 \lambda$, independent of its width w . The RF losses per square meter in the slab are

$$\frac{P_{fl}}{w^2} = \frac{1}{2} \cdot \frac{1}{\sigma_n \cdot \delta} \cdot \frac{1}{1 + [1/(\sigma_n \cdot \delta \cdot \omega \cdot \mu_0 \cdot \lambda)]^2} \cdot \left(\frac{B_{rf}}{\mu_0} \right)^2 \quad ,$$

from which we derive

$$R_{fl} = R_N \cdot \frac{1}{1 + [1/(\sigma_n \cdot \delta \cdot \omega \cdot \lambda)]^2} \quad ,$$

representing the surface resistance due to one individual fluxon. With the penetration depth δ of the nc electrons,

$$\delta = \sqrt{\frac{2}{\sigma_n \cdot \omega \cdot \mu_0}} \quad .$$

R_{fl} transforms into

$$R_{fl} = R_N \cdot \frac{1}{1 + (2\sigma_n \cdot \omega \cdot \mu_0 \cdot \lambda^2)^{-1}} \quad .$$

As $2\sigma_n \cdot \omega \cdot \mu_0 \cdot \lambda^2 \ll 1$, and $R_N = \sqrt{(\omega \cdot \mu_0 / (2 \cdot \sigma_n))}$, one ends up with

$$R_{fl} = (\omega \cdot \mu_0)^{3/2} (2 \cdot \sigma_n)^{1/2} \cdot \lambda^2 \quad .$$

The total average losses P per square meter consist of the losses of an individual fluxon summed over the number N of fluxons per square meter,

$$\frac{P}{w^2} = \frac{1}{2} \cdot \sum_{i=1}^N R_{fl} \cdot \left(\frac{B_{rf}}{\mu_0}\right)^2 = \frac{1}{2} \cdot N \cdot R_{fl} \cdot \left(\frac{B_{rf}}{\mu_0}\right)^2 \quad .$$

As the flux is (nearly) completely trapped upon cool down, the applied ambient flux B is redistributed in the form of fluxons the surface fraction of which is equal to B/B_{c2} . Hence

$$\frac{P}{w^2} = \frac{1}{2} \cdot \underbrace{\frac{B}{B_{c2}}}_{R_s} \cdot R_{fl} \cdot \left(\frac{B_{rf}}{\mu_0}\right)^2 = \frac{1}{2} \cdot \underbrace{R_{fl}}_{R_{fl}^0} \cdot B \cdot \left(\frac{B_{rf}}{\mu_0}\right)^2 \quad ,$$

defining the fluxon sensitivity R_{fl}^0 to

$$R_{fl}^0 = (\omega \cdot \mu_0)^{3/2} (2 \cdot \sigma_n)^{1/2} \lambda^2 \frac{1}{B_{c2}} \quad ,$$

which is eq. 3.

REFERENCES

- [1] C. J. Gorter and H. G. B. Casimir. Phys. Z. **35** (1934) 963; Z. Tech. Phys. **15** (1934) 539.
- [2] F. London, and H. London, H. Proc. Roy. Soc. **A149** (1935) 71.
- [3] J. Bardeen, L. N. Cooper, J. R. Schrieffer, Phys. Rev. **108** (1957) 1175.
- [4] W. Meissner and R. Ochsenfeld, Naturwiss. **21** (1933) 787.
- [5] D. Boussard and T. Linnecar, Proc. 1999 Cryogenic Engineering and International Cryogenic Materials Conference (CEC-ICMC'99), 12-16 July 1999, Montreal, Canada.
- [6] C. Benvenuti, S. Calatroni, I.E. Campisi, P. Darriulat, M.A. Peck, R. Russo, A.-M. Valente, Physica C **316** (1999) 153.
- [7] W. Weingarten, Physica C **339** (2000) 231-236.
- [8] W. Weingarten, Phys. Rev. STAB **14** (2011) 101002.
- [9] J. I. Gittleman and B. Rosenblum, Phys. Rev. Lett. **16** (1966) 734.
- [10] E. H. Brandt, Proc. 2nd Int. Workshop on Thin Films and New Ideas for Pushing the Limits of RF Superconductivity, INFN Laboratori Nazionali di Legano, Italy, 9 – 12 Oct. 2006.
- [11] Y. B. Kim, C. F. Hempstead, and A. R. Strnad, Phys. Rev. **139**, A1163 (1965).
- [12] C. C. Koch, J. O. Scarbrough, D. M. Kroeger, Phys. Rev. **B 9** (1974) 888.
- [13] N. Tsuda and T. Suzuki, J. Phys. Chem. Solids **28** (1967) 2487.
- [14] J. Halbritter, Journ. Appl. Phys. **97** (2005) 083904; M. A. Peck, Ph.D. thesis TU Wien, 1999.
- [15] C. Peroz and C. Villard, arXiv:cond-mat/0504104v1 [cond-mat.supr-con] 5 Apr 2005.
- [16] W. Weingarten, Proc. 1995 Workshop on RF Superconductivity, ed. B. Bonin, Gif-sur-Yvette, France, 17-20 Oct. 1995, p. 129.
- [17] P. Darriulat, C. Durand, P. Janot, N. Rensing, and W. Weingarten, P. Bosland, J. Gobin, and J. Martignac, ibid. ref. 16, p. 467.
- [18] S. Calatroni and R. Vaglio, Phys. Rev. STAB **22** (2019) 022001.
- [19] B. Piosczyk, P. Kneisel, O. Stoltz, and J. Halbritter, IEEE Trans. Nucl. Sci. **20** (1973) 108.
- [20] G. Arnolds-Mayer and W. Weingarten, IEEE Trans. Magn. **23** (1987) 1620.
- [21] M. Checchin, M. Martinello, A. Grassellino, S. Aderhold, S. K. Chandrasekaran, O. S. Melnychuk, S. Posen, A. Romanenko, and D. A. Sergatskov, Appl. Phys. Lett. **112** (2018) 072601.
- [22] A. Miyazaki and W. Venturini Delsolaro, arXiv:1812.04658.
- [23] C. Benvenuti, S. Calatroni, P. Darriulat, M. A. Peck, and A.-M. Valente, Physica C **351** (2001) 429.
- [24] M. Martinello, A. Grassellino, M. Checchin, A. Romanenko, O. Melnychuk, D. A. Sergatskov, S. Posen, and J. F. Zasadzinski, Appl. Phys. Lett. **109** (2016) 062601.
- [25] A. Grassellino, A. Romanenko, D. Sergatskov, O. Melnychuk, Y. Trenikhina, A. Crawford, A. Rowe, M. Wong, T. Khabiboulline and F. Barkov, Supercond. Sci. Technol. **26** (2013) 102001.
- [26] Georg Busch, Horst Schade, Lectures on solid state physics, Pergamon Press, Oxford, UK, 1976.
- [27] C. Camerlingo, P. Scardi, C. Tosello, R. Vaglio, Phys. Rev. **B31** (1985) 3121.
- [28] J. J. Hauser and H. C. Theuerer, Phys. Rev. **134** (1964) A198.